JACS
JOURNAL OF THE AMERICAN CHEMICAL SOCIETY

ARTICLE

pubs.acs.org/JACS

Screw Motion Regulates Multiple Functions of T4 Phage Protein Gene Product 5 during Cell Puncturing

Wataru Nishima,[†] Shuji Kanamaru,[‡] Fumio Arisaka,[‡] and Akio Kitao*[,†,§]

[†]Institute of Molecular and Cellular Biosciences, The University of Tokyo, 1-1-1 Yayoi, Bunkyo, Tokyo 113-0032, Japan

[‡]Graduate School of Bioscience and Biotechnology, Tokyo Institute of Technology, B-9, 4259 Nagatsuta, Midori-ku, Yokohama 226-8501, Japan

[§]Japan Science and Technology Agency, Core Research for Evolutional Science and Technology, 1-1-1 Yayoi, Bunkyo, Tokyo 113-0032, Japan

Supporting Information

ABSTRACT: Bacteriophage T4 penetrates the outer membrane of *Escherichia coli* using a multifunctional device composed of a gene product 5 (gp5) protein trimer. We report that gp5 sequentially exerts distinct functions along the course of penetration stages induced by screw motion. A triple-stranded β-helix of gp5 acts as a cell-puncturing drill bit to make a hole on the membrane and then send the lipids upward efficiently by strong charge interactions. The gp5 lysozyme domains, which degrade the peptidoglycan layer later, are shown to play novel roles to enlarge the hole and control the release of the β-helix. The lysozyme active site is protected from lipid binding during the penetration and is exposed after the β-helix release. Intrinsic multiple functions of gp5 are shown to be served in turn regulated by gradual change of interdomain interactions, which enables the initial infection process with single protein trimer by continuous screw motion. The results of lysozyme domain should be understood as the case where a single-function protein acquired multiple chemical functions through interplay with other domains in a multidomain protein.

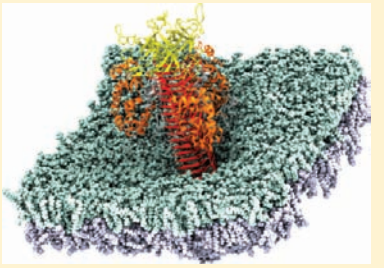

INTRODUCTION

Viruses possess efficient mechanism to infect a target cell. In the initial process of bacteriophage T4 infection of *Escherichia coli*, the protein complex of the gene product 5 (gp5) creates a channel on the outer membrane and degrades the peptidoglycan layer, which promotes injection of phage DNA into the cytoplasm.[1−6] A mature T4 phage comprises a head, a tail, and tail fibers (Figure 1A,B).[2] The tail consists of a baseplate and a double-cylindrical structure which is composed of the tail sheath and the tail tube attached to the baseplate.[7,8] Bacteriophage T4 infection is initiated by binding of the tail fibers to the lipopolysaccharide,[9] inducing contraction of the tail sheath. This process produces the force and transmits it to gp5 through the gp27 protein that is situated between the tail tube and gp5.[7,10,11] Monomers of the gp5 protein are assembled into a 3-fold symmetric trimer (Figure 1C). The gp5 complex is composed of the OB-fold domain (residues 1−129), linker1, the lysozyme domain (residues 174−339), linker2, and the β-helix domain (residues 389−575).[1]

The movement of gp5 during the penetration process has been deduced from a detailed structural analysis of the contractile tail sheath[7,11] based upon the assumption that the force generated by the sheath contraction is completely transmitted to gp5 through the tail tube. The sheath is composed of six helical strands, each of which has 23 subunits of gp18 protein which can also be viewed as a 23-stacked hexameric ring of gp18 ($6 \times 23 = 138$ subunits in total). The tail sheath first takes an extended form in relatively high energy state, then it undergoes conformational transition to lower energy contracted form, which produces the force to move gp5. Each layer of the six-subunit ring before and after contraction is 40.6 and 16.4 Å thick, respectively. Consequently, gp5 is expected to move 556.6 Å perpendicularly to the plane of the membrane and to rotate 345.4° in the counterclockwise direction viewed from the outside of the cell. The process of membrane penetration by gp5 is simulated by molecular dynamics simulation in this work. A lipid bilayer comprised of dioleyl phosphatidyl ethanolamine (DOPE) is arranged on the *xy*-plane of the simulation box and the symmetry axis of the gp5 trimer is initially placed along the *z*-axis in solution, 10 Å above the membrane (see Methods). After equilibration, the screw movement of gp5 is performed by applying force bias to the OB-fold domain, mimicking the effect of the force produced by the sheath. The penetration of gp5 into the membrane is simulated at vertical velocities of 5 Å/ns (Move1) and 10 Å/ns (Move2). Hereafter, gp5 position during the penetration will be specified by the moving distance from 0 to 300 Å. We have also performed the "Hold" simulations in quasi-equilibrium for force and torque evaluations.

METHODS

All the simulations were performed using the molecular simulation package NAMD[12] in NPT ensemble at 20 °C (293.15 K) and 1 atm with

Received: May 22, 2011
Published: July 27, 2011

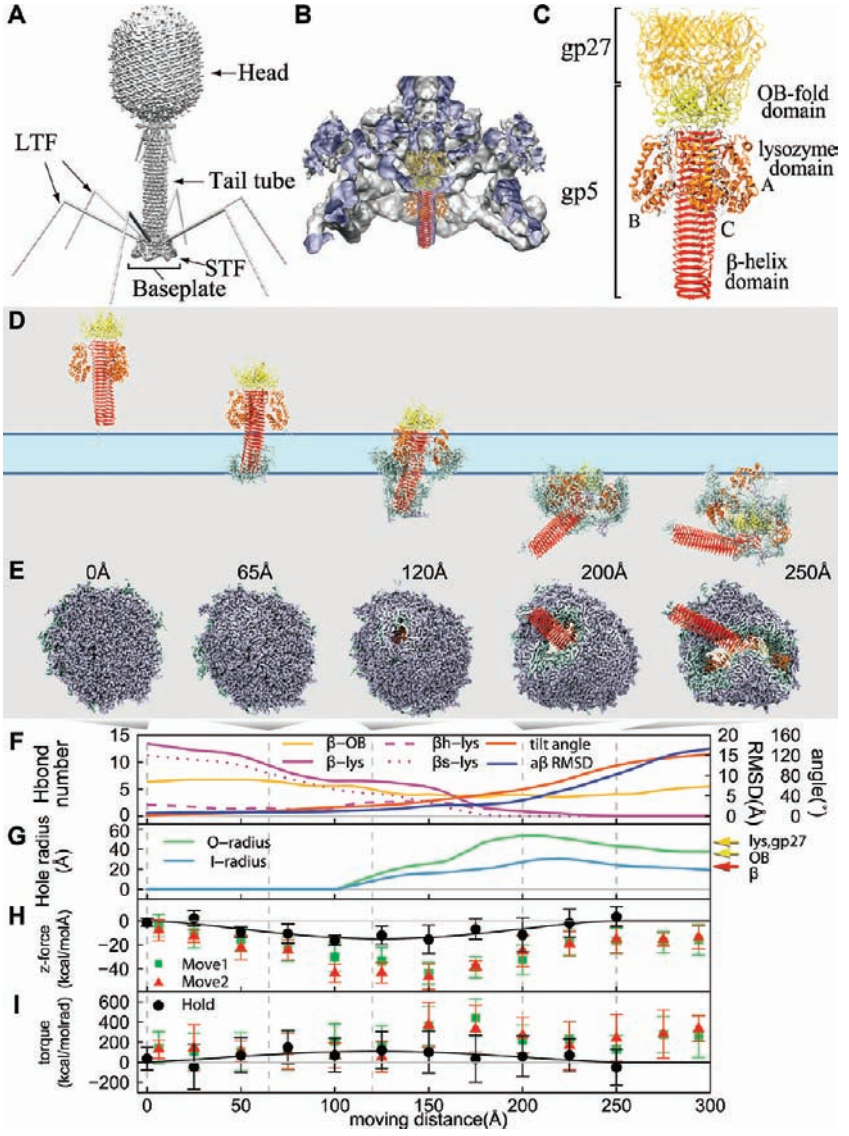

Figure 1. Series of events and changes of physical properties during the gp5 penetration. (A) Mature bacteriophage T4 structure from EM density maps.[32,7,8] (B) Cross section of the baseplate isosurface of the EM maps and the superimposed gp5−gp27 complex structure.[1] (C) The gp5−gp27 complex structure. The OB-fold (yellow), lysozyme (orange), β-helix domains (red), and two linkers (white) in gp5 and the gp27 trimer (gold). (D) Side view snapshots from the Move1 simulation (the zone in light blue shows the initial position of the membrane) and (E) bottom view. (F) The numbers of the hydrogen bonds between the β-helix and the OB-fold domains (β-OB); the β-helix and the lysozyme domains (β-lys); the β-helix region and the lysozyme domain (βh-lys); and between the antiparalell β-sheet region and the lysozyme domain (βs-lys) in Move1. The tilt angle between the β-helix and the z-axis; the C_α root-mean-square deviation of the β-sheet region from the crystal structure (aβ rmsd). (G) Radii of the outer (O-radius: green) and inner tangent (I-radius: blue) circles of the hole in Move1. (H) Force along z-axis and (I) torque.

the CHARMM27 force field.[13,14] The simulated systems were solvated with TIP3P water molecules[13] with 0.154 M NaCl to satisfy physiological concentration in the periodic boundary. The wild-type structure of gp5 (PDB ID: 1K28)[1] was adopted and gp5 missing residues 346−361 in linker2 was modeled based on the mutant S351L structure (PDB ID: 1WTH).[15] A gp5 trimer was first equilibrated in solution for 10 ns. Independently, a lipid bilayer consisting of 24 × 24 × 2 DOPE molecules in solution was equilibrated for 10 ns. Then, gp5 was combined with the DOPE system so that the distance between the bottom of the β-helix and the average position of the outer leaf phosphorus atoms along the z-axis was 10 Å within a box of approximately 178 × 178 × 272 Å^3. The system contains 885 242 atoms in total. We ensured that even at the end of the penetration simulations, gp5 was significantly apart from the periodic images of the membrane with this box size setup. During a 5 ns preparation run, positional restraints on the C_α atoms of the OB-fold domain were applied to maintain the gp5 position with a force constant of 2.0 kcal/(mol Å^2). In the production run, the reference coordinates for the OB-fold restraints were moved step-by-step to realize the screw motion of gp5 after equilibration for two distinct times (Move1, 400 ps; Move2, 200 ps). At each step, the reference coordinates were shifted 2 Å downward and rotated 1.24° in a counterclockwise direction viewed from the OB-fold. Total simulation times in Move1 and Move2 were 60 and 30 ns, respectively. In the end, the vertical position of the membrane plane defined by unperturbed lipids was shifted downward by approximately 30 Å in Move1 while the shift was negligible in Move2. Although the speed of the gp5 movement has not been experimentally measured at the molecular level, the simulated movement is likely to be faster than the real one. To examine

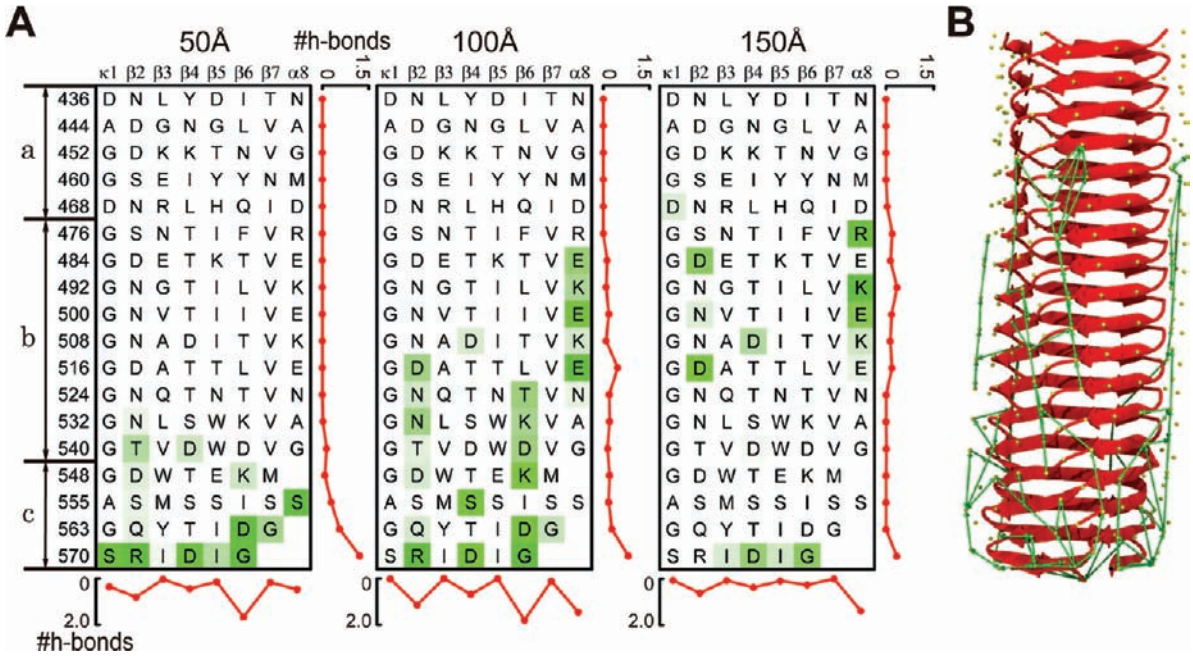

Figure 2. Hydrogen bonding pattern and lipid sliding path on the surface of the β-helix. (A) The hydrogen bonding between the β-helix of gp5 and the lipids for each amino acid of Hold simulations. The green shade represents the frequency. Red lines at bottom and right are the sum of the number of hydrogen bonds along the columns and rows, respectively. (B) Representative lipid sliding paths in the Move1 run (green arrows) on the surface of C_α atoms (yellow spheres).

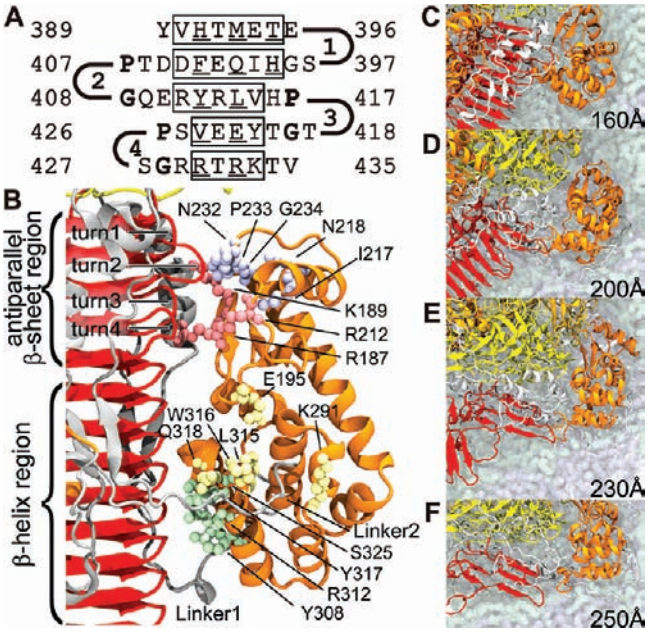

Figure 3. Interactions between lysozyme and β-helix domains and dissociation of the β-helix. (A) The residues in the antiparallel β-sheet region. (B) Structure of the β-helix and lysozyme domains. The inserted residues compared to T4L (blue) and residues interacting with the β-sheet (red), linker2 (yellow), and the β-helix (green). (C−F) The interactions between a lysozyme domain C in Figure 1C and the β-helix in Move1. The structure of gp27 (gold) is superimposed at the plausible position. (C) Dissociation of lysozyme, (D) the interaction between lysozyme and turn 2, (E) lysozyme dissociation, and (F) after complete breakage of the β-sheet.

possible artifacts caused by the differences in speed, we have also performed the simulation in quasi-equilibrium. We chose 11 snapshots from every 25-Å snapshots of the Move2 run between 0 and 250 Å and independently continued "Hold" simulations, keeping the position of the OB-fold for an additional 5 ns. Positional restraints onto the OB-fold domain were maintained for 5 ns in each Hold simulation. The figures were created by CHIMERA[16] (Figure 1A,B) and VMD[17] (Figures. 1C−E, 2B, 3B−F).

RESULTS

The Series of Events during Gp5 Penetration. The main events observed during gp5 penetration in Move1 are shown in Figure 1D,E and Supporting Information (SI) Figure S1 and Movies. As gp5 moves vertically over the distance between 0 and 60 Å, the β-helix strongly interacts with the head groups of the outer leaf lipids (SI Table S1 and SI Figure S2A,B). The tail-to-head directions of the outer leaf lipids are strongly steered toward the helix while the inner leaf lipids tend to keep their original orientations. At 63.5 Å, the first lysozyme domain makes contact with the lipids; at this moment, the β-helix has already slightly tilted (SI Table S2). At around 105 Å, a hole mostly covered with the lipid hydrophilic head groups is created (SI Figure S2B,C). During the moving distance around 120−150 Å, the hydrophilic hole slides on the side surface of the β-helix as gp5 penetrates. The lysozyme domains tightly interact with the outer leaf lipids, start to dissociate from the helix and enlarge the hole. At 250 Å, the β-helix domain is fully bent, breaking the structure of the antiparallel β-sheet on the top of this domain. The series of events in Move2 are almost identical to those in Move1 except for two points. In Move2, a slight bend of the β-helix domain alone is observed. Moreover, the timing of lysozyme dissociation from the β-helix is different (209 Å for Move2 but 230.5 Å for Move1). The latter is related to the stochastic rolling fluctuation of the lysozyme domain, which also changes the timing of initial contact of each lysozyme domain with the membrane.

Work for Membrane Penetration Is Comparable to Sheath Contraction Enthalpy. During the course of gp5 penetration, the total vertical force and torque applied onto the OB-fold domain are monitored (Figure 1H,I). The effects of the penetration speed were mainly seen in the force and torque. Although the force and torque in Hold were smaller than those in Move1 and Move2, the shape of the membrane was maintained in Hold. For the vertical force, the peak of the force are observed at 120 Å for Hold, and it corresponds to hole creation event. The maximum torque was observed at 123 Å. From the regression line for the results of Hold, work done by vertical force and torque are estimated to be 2065.4 and 173.1 kcal/mol, respectively (total work: 2238.5 kcal/mol). Since the driving force of gp5 is thought to be produced by the contraction of the sheath comprising 138 gp18 subunits,[7,10,11] the minimum enthalpy release upon urea-induced sheath contraction was experimentally estimated as 25 kcal/mol per gp18 monomer.[10] Therefore, the total enthalpy gain, 25 × 138 = 3450 kcal/mol, is roughly comparable to the work estimated in the simulation. On the basis of these data, the energy produced by sheath contraction is concluded to be sufficient to induce gp5 penetration.

Hole Creation on the Membrane and Lipid Sliding on the β-Helix Surface. The β-helix domain forms a triangular prism with a height of 110 Å and a width of 28 Å. The β-helix is known to be very stable, and is resistant to SDS denaturation at room temperature.[1,10] The β-helix domain contains three antiparallel β-sheets and a triple-stranded β-helix (Figures 2 and 3). The former consist of five β-strands (residues 389−435) and form the upper part of the prism directly interacting with the OB-fold and lysozyme domains (Figure 3A,B). In the middle of the triple-stranded β-helix, an 8-residue sequence motif VXGXXXXX is tandemly repeated 9 times starting from V482 (column β7 in Figure 2A) with G located on the lateral ridges of the prism (column κ1). The β-helix can be divided into three parts, region **a** (residues 436−475), **b** (residues 476−547), and **c** (residues 548−575). Regions **a** and **b** consist of one β-strand (β2−β7) and the edges (κ1 and α8). Region **a** is covered by the lysozyme domains and this coverage is maintained until the lysozyme domains strongly interact with the lipids and dissociate from the helix. Three out of the last four β-strands near the C-terminus (region **c**) have shorter strands, making the end of the prism sharper and narrower.

During the penetration process, the head groups of the lipid molecules strongly interact with the hydrophilic residues of the β-helix. In the initial stage (see 50 Å), the lipids mainly attach to the tip of the β-helix. Just before hole creation (100 Å), the surface of the elongated lipids covers the helix and some of the lipids slide onto the helix surface up to the middle of the β-helix. The positively and negatively charged residues located in the columns β2, β6, and α8 makes hydrophilic interactions with lipids, waters, and neighboring side chains. These interactions enable the sliding of the lipids on the helix surface, and maintain hydrophilic interactions with the helix while the lipids exchange partners. Considering the screw motion of gp5, the lipids first meet the residues in column β6, then β2, and finally α8 (Figure 2B). The lipids interact with the polar amino acid side chains but their downward moving speed is much slower than that of gp5. In this process, the lipids first slide on the helix surface along the polar-residue pattern, and are then handed over to the next pattern that is situated slightly upward on the helix surface. These three arrays of polar residues act to lift up the lipids relative to the helix, similar to the grooves in a twist drill bit.

The Process of Lysozyme Domain Dissociation. After initial contact with the lipids at around 63.5−95 Å, the lysozyme domains gradually exert other effects on the shape of the membrane as well as on the bend of the β-helix domain. The lysozyme domain has the well-known primary function of degradation of the peptidoglycan layer; however, it also plays the following additional roles that were discovered in this work. Compared to T4L (43% identity and 66% similarity), a total of five residues, I217-N218 and N232-P233-G234, are inserted (shown by the blue CPK in Figure 3B). Each lysozyme domain is situated on one ridge of the triangular prism of the β-sheet-β-helix, and also holds the two faces of the prism. It is noteworthy that a loop containing the gp5-inserted residues, N232-P233-G234, contacts with a turn (T406-P407-G408-Q409, turn 2 in Figure 3A) protruding from the β-sheet although they do not form a significant hydrogen bond. This contact may serve to stabilize the association of the lysozyme domain with the β-helix domain. The lysozyme domain initially interacts with three other regions of gp5, a part of the β-helix (green in Figure 3B), the antiparallel β-sheet (red), and a part of linker2 (yellow: also see SI Table S3). The first two regions are expected to stabilize the association of the lysozyme domain with the β-helix domain and prevent the opening of the active site cleft. Linker2 is bound to the expected peptidoglycan-binding site.[1] Dissociation of the lysozyme domains from these regions starts after landing on the membrane. The β-helix detaches first (Figure 3C), followed by detachment of the antiparallel β-sheet (Figure 3D−F) and finally the linker2 (also see SI Table S2).

Lysozyme Domains Enlarge the Hole. After dissociation from the antiparallel β-sheet, each lysozyme domain protrudes farther, supported solely by linker1 connection to the OB-fold domain. Each lysozyme strongly interacts with the lipids during the enlarging process of the hydrophilic hole. The radii of the created hole measured as inner and outer tangent circles (Figure 1G) reach the maximum values of 54.6 and 30.8 Å, respectively. This roughly fits to the maximum radius of gp27, 47 Å, and that of the tail tube, suggesting that the lysozyme domains also serve to enlarge the size of the hole. In the living cell, both gp5 and gp27 are synthesized together as a pair of trimers $(gp27-gp5)_3$.[18] Subsequently, gp5 undergoes post-translational cleavage at a peptide bond between 351 and 352 in linker2, and is cleaved into an N-terminal part (gp5*) consisting of the OB-fold and the lysozyme domains and a C-terminal part $(gp5C)_3$ containing the β-helix domain. This heterononameric assembly $(gp27-gp5^*-gp5C)_3$ is stabilized by a noncovalent bond. At high temperature, it dissociates into $(gp27-gp5^*)_3$ and $(gp5C)_3$; however, the gp27−gp5* interaction is more stable. In this simulation, gp27 is not included; the possible position of gp27 can be deduced by superimposing the gp27 structure just above the OB-fold domain based on the gp5−gp27 co-crystal structure (Figure 1C). Gp27 should serve to maintain the hole size and may also play an additional role of pushing the lysozyme domains into the inter membrane space. Interestingly, the created hydrophilic hole maintains a hatch shape similar to the hole (SI Figure S3), which might be used for prompt repair of the hole as the hole on the outer membrane is known to be repaired after the injection of phage DNA.[19]

We also observed that the active sites are protected from the binding of lipids, even after the dissociation from the β-helix. The peptidoglycan binding site is located on the exposed surface; however, it is protected by the direct binding of linker2 until the final stage of the lysozyme release.

Bending Mechanism of the β-Helix Domain. For effective injection of phage DNA, the β-helix domain (gp5C) is expected to be removed from the created hole, because the substrate-binding sites of the lysozyme domain are then opened and lysozyme activity increases at least 10-fold.[15] To explain this effect, dissociation of gp5C has been proposed.[2] The aforementioned bend of the β-helix domain starts from the antiparallel β-sheet. The increase of the tilt angle relative to the *z*-axis significantly (Figure 1F) correlates with the increase of the root-mean-square deviation of the β-sheet compared to the initial structure as well as with the decreased interactions between the lysozyme and the β-helix domains. Before contact of the lysozyme domains with the lipids, the β-helix domain has been slightly tilted solely due to interactions with the outer leaf lipids. At this stage, the lysozyme domains follow the tilt of the β-helix, maintaining the interdomain contacts with the aforementioned three regions of the β-helix domain. Although the dynamic behavior of the lysozyme domain in equilibrium (before penetration) is nearly symmetric around the 3-fold axis, the dynamics of each subunit during the penetration process does not occur either concomitantly or symmetrically. Lysozyme C on the opposite side of the tilt is the first to make contact with the lipids, being attracted to the tilted β-helix and being situated closest to the membrane.

Turns 1−4 that connect five β-strands are located at two ridges of the triangular prism (Figure 3A). Turns 2−4 contain either a PG or a PXG pattern, a highly flexible motif that can undergo "peptide-plane flip".[20] Each lysozyme domain tightly holds turns 1 and 3 of the same subunit and turns 2 and 4 of another subunit with hydrogen bonds. R187, K189, and R212 in all of the lysozyme domains commonly interact with the β-sheet region. Interestingly, these residues exchange their hydrogen bonding partner along the course of gp5 penetration. R187 and K189 of lysozyme A sequentially exchange their hydrogen-bonding partners from turns 3 to 2, and then to 1 and from turn 2 to 1, respectively. R212 of lysozyme A maintains interactions with the relatively protruding turn 2 until dissociation. Similarly, R187 and K189 of Lysozyme B exchange their partners from turns 3 to 2 and 2 to 1, respectively, while R212 of lysozyme B maintains the hydrogen bond with turn 2. Lysozyme C located underneath the β-helix shows more complicated sliding interactions (Figure 3C−E). R187 initially interacts with T418 of turn 3, then slides step by step to turns 2, 1, and Y389 in the N-terminal side of the first β-strand, while K189 and R212 mostly interact with turn 2. G319 continues the interaction with Q409 in protruding turn 2 until dissociation (Figure 3E). Just below this turn, the hydrogen bond between the third and fourth β-strands of subunit B and those between the second and third β-strand of subunit C are broken and a large bend starts from this point. Although a large bend did not occur in Move2, a similar tendency was also observed. To examine amino acid sequence conservation of gp5, we conducted homology analysis of gp5-like proteins among T4-like bacteriophage family, T4, RB69, RB49, Aeh1, 44RR2.8t, and KVP40. Since KVP40 does not have the lysozyme domain,[21] it was excluded from the homology analysis of the lysozyme domain region but was considered in the other cases. The conservations of the aforementioned key residues, R187, K189, R212, G319, Y389, Q409, and T418 were found to be 100.0, 40.0, 80.0, 100.0, 100.0, 66.7, and 33.3%, respectively. The average conservation of the PG motif[20] is 88.9%, which might be due to structural constraints to the turn structures. Interestingly, the sequence conservations of the lysozyme domain (72.2%) and the antiparallel β-sheet region (76.6%) are higher than those of the OB-fold domain (67.1%) and the β-helix region (57.6%).

At the beginning of penetration, the lipid head groups slide on the surface of the β-helix, and then tightly bind to the lysozyme domains. When a large bend is observed, the lipids bound to the β-helix tend to show greater dissociation, allowing larger movement of the helix. Not only the lysozyme domains, but also linker1 and linker2 effectively function as lipid binding receptors, thereby promoting the bend of the β-helix.

CONCLUSION

In this study, we reported that a protein gp5 trimer sequentially exerts distinct multiple functions induced by screw motion. A triple-stranded β-helix of gp5 not only acts as a cell-puncturing drill bit to make a hole on the membrane, but also serves to send the lipids upward efficiently by strong charge interactions with the charged side chains situated on the surface of the helix. We also showed that the gp5 lysozyme domains play novel roles to enlarge the hole of the membrane and control the release of the β-helix. Interestingly, the lysozyme active site is protected from lipid binding during the penetration and is exposed after the β-helix release, suggesting the prompt enzymatic function to degrade peptidoglycan layer after penetration of the outer membrane. These intrinsic multiple functions were shown, in turn, to be regulated by gradual change of interdomain interactions. This concerted and sequential mechanism enables the initial infection process with single protein trimer by continuous screw motion.

If gp5-like proteins do not contain lysozyme domain as in KVP40 (close relative of T4 phage)[21] and as in VgrG-related proteins in type VI secretion system of *Vibrio cholerae*,[22,23] the penetration could be less effective because of not only the lack of the lysozyme activity to degrade the peptidoglycan layer, but also the lack of support to stabilize the β-helix and hole enlargement function. In this case, the gp27 attached to the OB-fold domain should serve to enlarge the hole. It is also worthwhile considering possible effects of the β-helix length variations. The distance from the lower tip of the β-helix to the bottom of the lysozyme domain is 54 Å, which is longer than the membrane thickness of ∼30 Å. However, the timings of the lysozyme landing (63.5−95 Å) and the hole creation (105 Å) are not largely different. If the β-helix is much shorter, it will lose the structural support by the lysozyme domains earlier because the lysozymes land on the membrane earlier than the hole creation, which can make the β-helix more mobile and the penetration less efficient. If the β-helix is much longer, it will be stable even after the hole creation and the lysozyme release will be delayed, which can also alter the penetration process to be less efficient. This consideration suggests that the length of the β-helix is in the optimal range.

We found that the exchange of hydrogen bonding partners between the lipid head groups and the β-helix, and that between the lysozyme domains and β-sheets, serves as an essential mechanism to allow large low-energy structural changes. Similar "sliding interaction" has also been observed in bacterial flagella.[24−26] During the supercoiling transitions of the flagellar filament and hook, significant interface sliding between protein subunits is expected. To avoid large energy loss due to the sliding, the interaction was maintained by similar properties of amino acid (i.e., hydrophilic or hydrophobic) with variable partner in the different type of supercoil structures. Such "sliding

interaction" might be a common mechanism for maintaining intermolecular interaction during large conformational changes in supramolecular systems.

In this work, the model lipid bilayer is composed of DOPE alone while the membrane of *E. coli* contains a mixture of several components, for example, phosphatidylethanolamine (PE), 75−85%; phosphatidylglycerol (PG), 10−20%; and cardiolipin (CL), 5−15%.[27] Lipopolysaccharide (LPS) and membrane protein could also affect the membrane property. Since LPS helps to stabilize the overall membrane structure,[28] the penetration energy could be underestimated in this work. Although the membrane composition of *E. coli* and the present simulation are different, the penetration of a real *E. coli* membrane by gp5 is expected to take place similarly, because the observed events are mainly caused by the intrinsic nature of gp5 and features that are common to other types of lipids. To perform simulation with a more realistic membrane, multicomponent membrane should be prepared in the future. Because of the heterogeneity of the system, longer simulations with multiple trials should be carried out. In a real system, the peptidoglycan layer is located inside of the outer membrane. There are several uncertainties regarding the distance between the outer membrane and the peptidoglycan layer. Although the distance between the outer membrane and the peptidoglycan layer is not well-known, it is believed to be shorter than the moving distance of the simulation.[29−31] If the β-helix contacts with the peptidoglycan layer in the middle of penetration, this would be expected to strongly promote bending. It is also unclear if gp5 is located at the tip of the tail tube. On the basis of the gp5−gp27 complex structure superimposed on the EM density map of the baseplate, gp5 is at the tip when lysozyme density is absent (Figure 1B).[1] If not, there might be other subunits (possibly gp26) at the tip of gp5.[4]

■ ASSOCIATED CONTENT

Supporting Information. Three figures for the cell punctual process, deformed lipids and structure of lipid bilayer, 3 tables about interactions and events, complete ref 13, as well as 3 different angles of simulation movies (mpg files). This material is available free of charge via the Internet at http://pubs.acs.org.

■ AUTHOR INFORMATION

Corresponding Author
kitao@iam.u-tokyo.ac.jp.

■ ACKNOWLEDGMENT

This work was supported by the Next Generation Super Computing Project, Nanoscience Program and Computational Material Science Initiative, Grant-in-Aid for Scientific Research (B) from JSPS to A.K. and Grants-in-Aid for Scientific Research on Priority Areas from MEXT to S.K., F.A., and A.K. The simulations were mainly done at the Research Center for Computational Science, Okazaki Research Facilities, National Institutes of Natural Sciences.

■ REFERENCES

(1) Kanamaru, S.; Leiman, P. G.; Kostyuchenko, V. A.; Chipman, P. R.; Mesyanzhinov, V. V.; Arisaka, F.; Rossmann, M. G. *Nature* **2002**, *415*, 553.
(2) Leiman, P. G.; Kanamaru, S.; Mesyanzhinov, V. V.; Arisaka, F.; Rossmann, M. G. *Cell. Mol. Life Sci.* **2003**, *60*, 2356.
(3) Leiman, P. G.; Chipman, P. R.; Kostyuchenko, V. A.; Mesyanzhinov, V. V.; Rossmann, M. G. *Cell* **2004**, *118*, 419.
(4) Rossmann, M. G.; Mesyanzhinov, V. V.; Arisaka, F.; Leiman, P. G. *Curr. Opin. Struct. Biol.* **2004**, *14*, 171.
(5) Kanamaru, S.; Gassner, N. C.; Ye, N.; Takeda, S.; Arisaka, F. *J. Bacteriol.* **1999**, *181*, 2739.
(6) Nakagawa, H.; Arisaka, F.; Ishii, S. *J. Virol.* **1985**, *54*, 460.
(7) Kostyuchenko, V. A.; Chipman, P. R.; Leiman, P. G.; Arisaka, F.; Mesyanzhinov, V. V.; Rossmann, M. G. *Nat. Struct. Mol. Biol.* **2005**, *12*, 810.
(8) Kostyuchenko, V. A.; Leiman, P. G.; Chipman, P. R.; Kanamaru, S.; van Raaij, M. J.; Arisaka, F.; Mesyanzhinov, V. V.; Rossmann, M. G. *Nat. Struct. Biol.* **2003**, *10*, 688.
(9) Crawford, J. T.; Goldberg, E. B. *J. Mol. Biol.* **1980**, *139*, 679.
(10) Arisaka, F.; Engel, J.; Klump, H. *Prog. Clin. Biol. Res.* **1981**, *64*, 365.
(11) Aksyuk, A. A.; Leiman, P. G.; Kurochkina, L. P.; Shneider, M. M.; Kostyuchenko, V. A.; Mesyanzhinov, V. V.; Rossmann, M. G. *EMBO J.* **2009**, *28*, 821.
(12) Phillips, J. C.; Braun, R.; Wang, W.; Gumbart, J.; Tajkhorshid, E.; Villa, E.; Chipot, C.; Skeel, R. D.; Kale, L.; Schulten, K. *J. Comput. Chem.* **2005**, *26*, 1781.
(13) MacKerell, A. D.; et al. *J. Phys. Chem. B* **1998**, *102*, 3586.
(14) MacKerell, A. D., Jr.; Banavali, N.; Foloppe, N. *Biopolymers* **2000**, *56*, 257.
(15) Kanamaru, S.; Ishiwata, Y.; Suzuki, T.; Rossmann, M. G.; Arisaka, F. *J. Mol. Biol.* **2005**, *346*, 1013.
(16) Pettersen, E. F.; Goddard, T. D.; Huang, C. C.; Couch, G. S.; Greenblatt, D. M.; Meng, E. C.; Ferrin, T. E. *J. Comput. Chem.* **2004**, *25*, 1605.
(17) Humphrey, W.; Dalke, A.; Schulten, K. *J. Mol. Graphics* **1996**, *14*, 33.
(18) Arisaka, F.; Kanamaru, S.; Leiman, P.; Rossmann, M. G. *Int. J. Biochem. Cell Biol.* **2003**, *35*, 16.
(19) Duckworth, D. H. *Bacteriol. Rev.* **1970**, *34*, 344.
(20) Nishima, W.; Qi, G. Y.; Hayward, S.; Kitao, A. *Bioinformatics* **2009**, *25*, 628.
(21) Nemoto, M.; Mio, K.; Kanamaru, S.; Arisaka, F. *J. Bacteriol.* **2008**, *190*, 3606.
(22) Mekalanos, J. J.; Pukatzki, S.; Ma, A. T.; Revel, A. T.; Sturtevant, D. *Proc. Natl. Acad. Sci. U.S.A.* **2007**, *104*, 15508.
(23) Leiman, P. G.; Basler, M.; Ramagopal, U. A.; Bonanno, J. B.; Sauder, J. M.; Pukatzki, S.; Burley, S. K.; Almo, S. C.; Mekalanos, J. J. *Proc. Natl. Acad. Sci. U.S.A.* **2009**, *106*, 4154.
(24) Samatey, F. A.; Matsunami, H.; Imada, K.; Nagashima, S.; Shaikh, T. R.; Thomas, D. R.; Chen, J. Z.; DeRosier, D. J.; Kitao, A.; Namba, K. *Nature* **2004**, *431*, 1062.
(25) Kitao, A.; Yonekura, K.; Maki-Yonekura, S.; Samatey, F. A.; Imada, K.; Namba, K.; Go, N. *Proc. Natl. Acad. Sci. U.S.A.* **2006**, *103*, 4894.
(26) Furuta, T.; Samatey, F. A.; Matsunami, H.; Imada, K.; Namba, K.; Kitao, A. *J. Struct. Biol.* **2007**, *157*, 481.
(27) Raetz, C. R. *Microbiol. Rev.* **1978**, *42*, 614.
(28) Yethon, J. A.; Heinrichs, D. E.; Monteiro, M. A.; Perry, M. B.; Whitfield, C. *J. Biol. Chem.* **1998**, *273*, 26310.
(29) Matias, V. R.; Al-Amoudi, A.; Dubochet, J.; Beveridge, T. J. *J. Bacteriol.* **2003**, *185*, 6112.
(30) Vollmer, W.; Seligman, S. J. *Trends Microbiol.* **2010**, *18*, 59.
(31) Vollmer, W.; Blanot, D.; de Pedro, M. A. *FEMS Microbiol. Rev.* **2008**, *32*, 149.
(32) Fokine, A.; Chipman, P. R.; Leiman, P. G.; Mesyanzhinov, V. V.; Rao, V. B.; Rossmann, M. G. *Proc. Natl. Acad. Sci. U.S.A.* **2004**, *101*, 6003.